Earth's Future

RESEARCH ARTICLE
10.1029/2022EF002809

Observational Evidence for Multivariate Drought Hazard Amplifications Across Disparate Climate Regimes

Poulomi Ganguli[1], **Avijit Majhi**[1], **and Rohini Kumar**[2]

[1]Agricultural and Food Engineering Department, Indian Institute of Technology Kharagpur, Kharagpur, India, [2]Department of Computational Hydrosystems, Helmholtz-Centre for Environmental Research–UFZ, Leipzig, Germany

Key Points:

- Global synthesis of multivariate drought imprints between rain-deficit and streamflow droughts
- Observational assessment showed strong amplifications in bivariate drought hazards to dependence
- Strong imprints between rain-deficit and streamflow droughts in transitional sub-tropics

Supporting Information:

Supporting Information may be found in the online version of this article.

Correspondence to:

P. Ganguli and R. Kumar,
pganguli@agfe.iitkgp.ac.in;
rohini.kumar@ufz.de

Citation:

Ganguli, P., Majhi, A., & Kumar, R. (2022). Observational evidence for multivariate drought hazard amplifications across disparate climate regimes. *Earth's Future*, *10*, e2022EF002809. https://doi.org/10.1029/2022EF002809

Received 31 MAR 2022
Accepted 11 JUL 2022

Author Contributions:

Conceptualization: Poulomi Ganguli, Rohini Kumar
Data curation: Poulomi Ganguli
Formal analysis: Poulomi Ganguli, Avijit Majhi
Investigation: Poulomi Ganguli, Avijit Majhi
Methodology: Poulomi Ganguli, Rohini Kumar
Project Administration: Poulomi Ganguli, Rohini Kumar
Software: Poulomi Ganguli
Supervision: Poulomi Ganguli, Rohini Kumar
Validation: Avijit Majhi

Abstract Drought poses significant challenges to global water security in a warming world. A global-scale synthesis of the multivariate drought risk considering interdependencies between drought attributes across disparate climate regimes is still lacking. Leveraging precipitation and streamflow observations of 270 large catchments over the globe, we show that multivariate drought hazard amplifies significantly (at ~65–76% of catchments) considering dependence between drought duration and severity. A signifying nature of this amplification (A) is the power-law scaling with dependence metric ($A \propto \tau^{\lambda}$; $\lambda = 5 - 12$; where τ and λ are Kendall's correlation and the scaling exponent), revealing current approaches considering drought attributes as independent or linearly dependent will severely underestimate likelihood of extreme droughts. Furthermore, we find disparate responses in the multivariate imprints of meteorological to hydrological droughts across climate types, with strengths varying from large to modest in Tropics and Mid-latitudes, which indicates weaker overlap between rain-deficit and streamflow droughts. In contrast, a strong overlap in multivariate hazards of rain-deficit and streamflow droughts is apparent across transitional Subtropics. Our study highlights the relevance of accounting for multivariate aspects of drought hazards to inform adaptation to water scarcity in a changing climate.

Plain Language Summary The world's large river basins support a huge population and diverse ecosystems. A growing body of the literature suggests holistic risk management requires a "multivariate event perspective" to analyze interacting drought attributes rather than each of these drivers in isolation. Using the gauge-based observational framework, we show a robust amplification in multivariate drought hazard and this response co-vary among distinct climate regimes. Our multivariate hazard framework shows a contrasting response in multivariate imprints (or degree of overlap) of rain-deficit (drivers) to streamflow (response)-droughts across disparate climate regimes for milder and extreme categories of droughts; from substantial regional variations in multivariate drought hazard in tropics and mid-latitudes, revealing a weak imprint between drought types. In contrast, the transitional subtropics show a modest variation in the multivariate imprint of drought types, indicating stronger imprint. We emphasize that failure to account for nonlinear interactions among interacting drought attributes will severely underestimate the extreme drought hazard, jeopardizing the adequacy of resilient water infrastructure design. The insights will aid in adaptation to extreme droughts under global warming.

1. Introduction

Droughts are slowly developing natural disasters that have caused $29 billion of damages in agricultural sectors between 2005 and 2015 and have affected more than 390 million people globally in 2016 (FAO, 2018; Guha-Sapir et al., 2017). The intensity and frequency of droughts are expected to exacerbate with climate warming in observations and model simulations (Trenberth et al., 2014), affecting changes in water availability at large-scales (Greve et al., 2018; Schewe et al., 2014). While a prolonged precipitation deficit often triggers drought onset, very few studies (Apurv et al., 2017; Gevaert et al., 2018; Van Loon et al., 2014) have focused on propagation (Van Loon, 2015) of droughts (*i.e.*, translation from one type to another) on a global or hemispherical scale, however, a few local to national scale assessments are available (Brunner & Tallaksen, 2019; Haslinger et al., 2014; Van Loon & Laaha, 2015). Accumulating evidences (Hao & Singh, 2015) suggests that it is hard to distinguish responses to different categories of droughts, which may co-occur simultaneously or in close succession (*e.g.*, meteorological drought is typically preceded by hydrological drought) and are interconnected in nature. In particular, a growing body of the literature (AghaKouchak et al., 2014; Ganguli & Ganguly, 2016; Hao & Singh, 2015) reveals for

Visualization: Avijit Majhi
Writing – original draft: Poulomi Ganguli
Writing – review & editing: Poulomi Ganguli, Rohini Kumar

precise risk management; a "multivariate event perspective" (Raymond et al., 2020) is required to characterize the interdependent drought attributes, such as severity and duration, and their interlinkage, especially for extremes.

While in recent years, the growing number of literature has focused on multivariate drought hazard assessments (Chang et al., 2016; Cheng et al., 2015; Gu, Chen, Yin, Xu, & Chen, 2020; Gu, Chen, Yin, Xu, & Zhou, 2020) at a local or national scale (Ganguli & Ganguly, 2016; Sahana et al., 2020), a quantitative understanding of their multivariate imprints considering interdependence between attributes from the preconditioned driver (meteorological droughts) into responder hazard (hydrological droughts) at a global scale remains unexplored (See Figure 1 for details). Here the multivariate perturbation of stimuli, for example, meteorological drought, could potentially affect the responder drought type in close succession of a time window through the mechanism of pooling (*i.e.*, merging meteorological drought into a persistent hydrological drought) and lengthening (*i.e.,* increase in drought persistency moving from meteorological-soil moisture depletion-to hydrological) (Van Loon et al., 2014). Further, most of the literature on multivariate drought hazard assessments has primarily analyzed a single type of drought, such as either meteorological (Das et al., 2020; Dixit & Jayakumar, 2021; Mirabbasi et al., 2012; Poonia et al., 2021; Shiau, 2006) or streamflow-based (Kao & Govindaraju, 2010; Wang et al., 2020) droughts. The imprints of precipitation deficit onto streamflow droughts across different climate regimes of the globe considering mutually dependent drought attributes and its response to milder versus extreme droughts remains unclear.

Observational analyses of local-scale drought assessments (Brunner & Tallaksen, 2019; Gu, Chen, Yin, Xu, & Chen, 2020; Gu, Chen, Yin, Xu, & Zhou, 2020; Haslinger et al., 2014; Oertel et al., 2018) are often limited to small to medium-sized catchments (*e.g.*, 100–1000 km^2) or covering limited periods (*e.g.*, 30–40 years). A few of these studies have investigated the characteristics of low flow indicators from observations or stochastically simulated discharge time series (Brunner & Tallaksen, 2019; Van Loon & Laaha, 2015). In contrast, others focused on standardized indices of monthly hydrometeorological variables, such as either streamflow or precipitation, evapotranspiration, and/or their combinations (Gevaert et al., 2018; Haslinger et al., 2014; Oertel et al., 2018). To summarize, the spatial and temporal heterogeneity of regional-scale assessments complicate the generalizability of observed imprints of one drought type onto another, globally. To better assess changes in different aspects of drought hazards under global warming across disparate climatic regimes, it is essential to investigate and understand robust inferences of observed changes in extreme drought dynamics over a relatively long period.

Second, at a large scale, very few studies (Apurv et al., 2017; Gevaert et al., 2018; Van Loon et al., 2014) have assessed drought propagation and found translation mechanisms of meteorological (characterized by below-normal rainfall) to hydrological (characterized by below-normal streamflow) droughts are primarily controlled by climate and catchment properties. Using 1271 virtual catchments differing only on climate types, Van Loon et al. (2014) studied the relationship between modeled drought duration and severity over 27 Köppen-Geiger sub-climate zones based on a lumped conceptual, Hydrologiska Byråns Vattenbalansavdelning (HBV) model. Extending this work, using numerical experiments with a simple water balance model, Apurv et al. (2017), reported the effect of climate types on drought propagation in both natural and anthropogenically altered catchments. Gevaert et al. (2018) have investigated the timescales of drought propagation in seasonal drought types, that is, both summer and winter, using an ensemble of global hydrological models. However, all these large-scale assessments (Apurv et al., 2017; Gevaert et al., 2018; Van Loon et al., 2014) have relied on simple water balance models. Although large-scale hydrologic models can reasonably simulate the average annual low and high flows, they tend to over/underestimate the frequency of dry anomalies and associated extremes (Clark et al., 2008, 2011; Dankers & Feyen, 2009; Lehner et al., 2006; Stahl et al., 2011). Recently, Gu, Chen, Yin, Xu, & Chen (2020) investigated the bivariate hazard transferability from meteorological to hydrological droughts using an index "Drought hazard propagation ratio (DHPR)" from three Chinese catchments across two significant rivers, Yangtze and Yellow River basins. However, the analysis used only one particular climate type with a limited number of station records, leading to the generalizability of multivariate drought propagation patterns across different climate types mainly deemed unexplored.

Third, although droughts are multidimensional, encompassing several interacting attributes, most of the earlier assessments have considered the propagation of drought responses considering changes in individual drought characteristics (e.g., severity, duration; Gevaert et al., 2018). A few studies (Van Loon et al., 2014) have considered a linear relationship to understand the propagation of streamflow droughts across different climate regimes by fitting a linear regression line over log-transformed bivariate streamflow drought attributes, deficit volume and

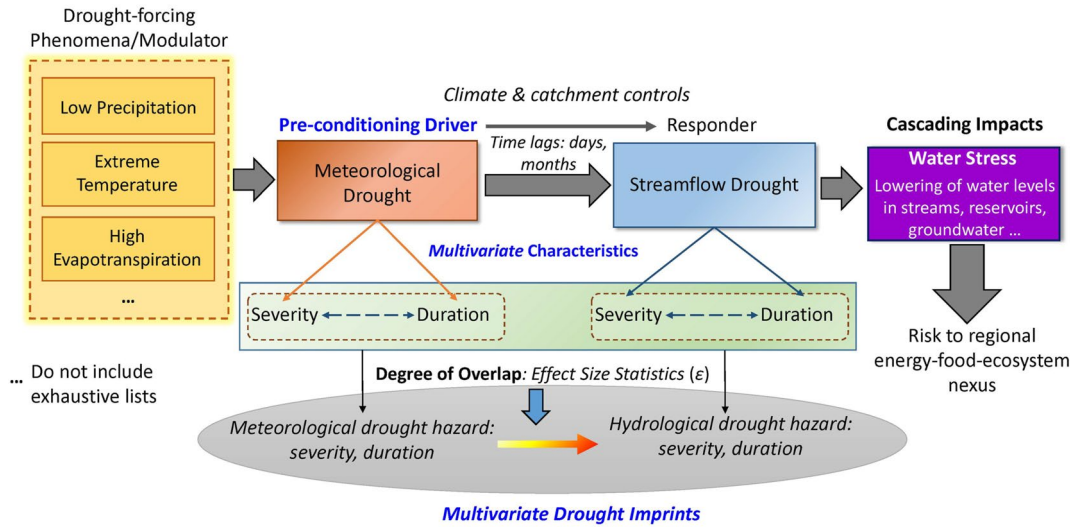

Figure 1. Multivariate imprints of meteorological to hydrological droughts. The coupling strength between drought types are determined using effect size statistics of bivariate hazards accounting for dependence between severity and duration (see Methods: Section 2.7 for details). An arrow indicates possible causal links between interacting variables.

duration. Although a scaling relationship between hydroclimatic variables is typically established in the literature (Markonis & Koutsoyiannis, 2016; O'Gorman & Schneider, 2009; Wyżga et al., 2020), little is known about any scaling relationship between bivariate drought hazard and the dependence between underlying drought attributes across river basins in different climate regimes.

Multivariate drought risk may emerge from two distinct mechanisms (see Figure 1). First, meteorological droughts, which result from prolonged rain deficit together with extreme temperature and/or high evapotranspiration (drought-forcing phenomena), act as a precursor/preconditioning (Van Loon & Laaha, 2015) driver for catchment-scale hydrological droughts (a responder). Severe meteorological droughts combined with synoptic-scale circulations and catchment-scale geomorphological conditions, such as atmospheric blocking and base flow (or catchment-scale soil moisture/snow memory), may amplify the translation of hydrological droughts. Second, the imprints of multidimensional droughts considering correlated multiple hazards have received little attention in drought propagation analysis (Gevaert et al., 2018; Van Loon et al., 2014). For example, the severe and longer (or average duration) meteorological droughts may affect the propagation timing of persistent catchment-scale streamflow droughts across different climate regimes (Leonard et al., 2014).

Using 270 observed streamflow records, here we present a systematic and probabilistic assessment of global scale multivariate drought imprints (Figure 2a; Table S1 in Supporting Information S1). To maximize spatiotemporal coverage, we consider only large river basins of basin area 20,000 km^2 or more and mean annual discharge is equal to or excess of 100 m^3/s (see definition: Methods and Text S1 in Supporting Information S1) with periods of record availability of 60 years or more. We consider three dominant climate regions over the globe (Najibi & Devineni, 2018): Tropics (23.5°N to 23.5°S), Subtropics (23.5° N to 35°N and 23.5° S to 35°S), and Mid-Latitudes (35° N to 60° N and 35° S to 60° S) in our analysis. Specifically, we seek to address the following questions: (a) what would be the multivariate response of droughts for milder versus extreme events considering dependence between attributes? (b) Among the three dominant climate regions, which one is the drought hotspot showing the slower or faster translation of one drought type into another and prone to a persistent drought? Using global scale historical streamflow and precipitation observations, we investigate multivariate imprints of meteorological to hydrological droughts across the world's large river basins in a copula-based dependence framework, considering interdependence between different drought attributes (See Methods and also Figure S1 in Supporting Information S1 for the workflow). Using this framework, we also quantify the change ("signal") – to –variability ("noise") of multivariate drought hazard for milder (or low; *i.e.*, joint exceedance of tenth percentiles of drought attributes, severity and duration) and extreme (high; joint exceedance of 90th percentiles of severity and duration) droughts to detect hotspot climate regimes that might be prone to persistent deficits. We analyse meteorological and hydrological droughts using the standardized indices of precipitation and streamflow time series

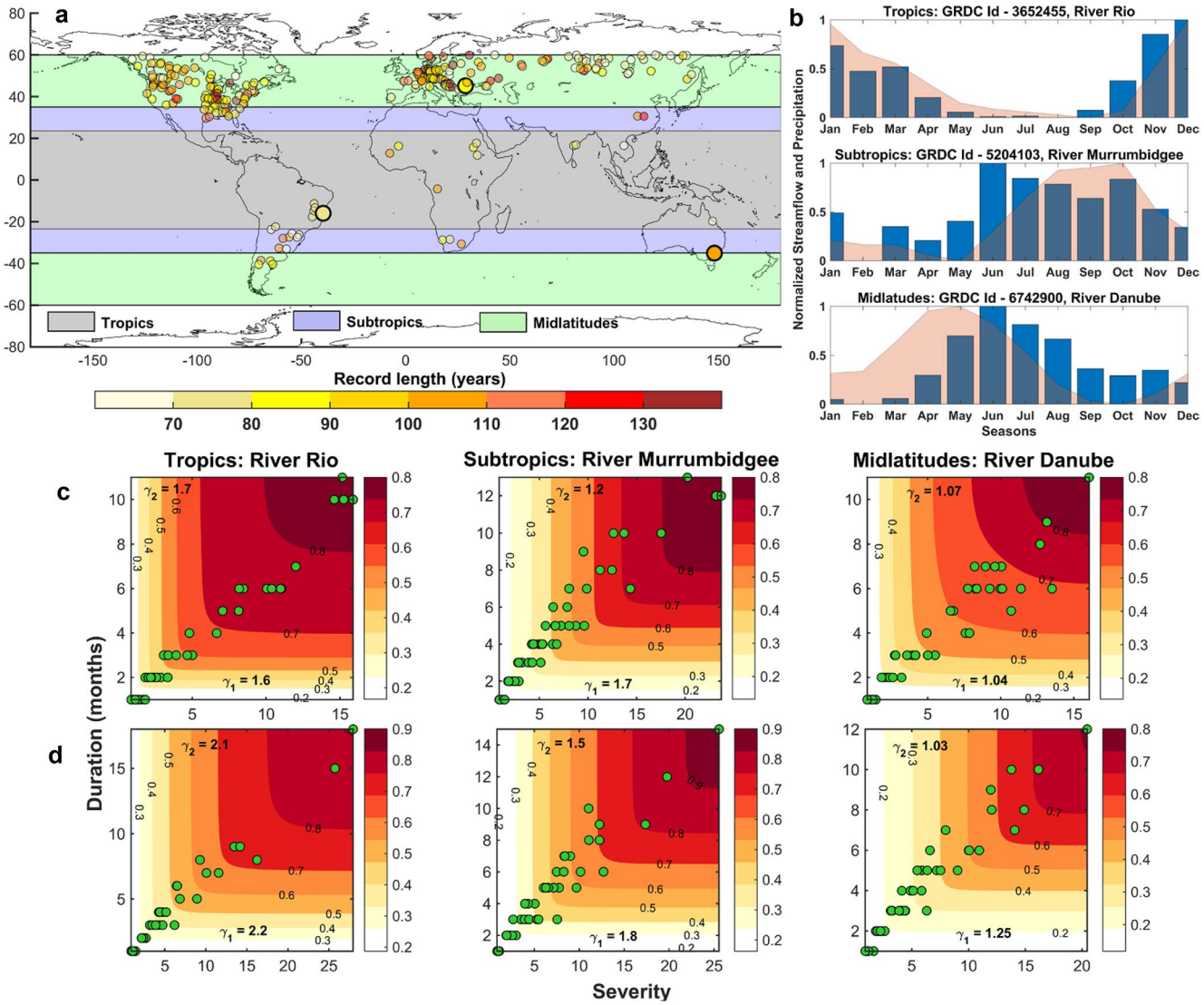

Figure 2. (a) Spatial distributions of streamflow gauges across three climatic regions, tropics, subtropics, and mid-latitudes. Shading of circles indicates the available record lengths. The representative sites from three climate regimes are marked with bigger circles. (b) Normalized mean monthly flow patterns (in red color) and precipitation (in blue vertical bars) of three representative stations from three climate regimes. We perform normalization (within the range 0–1) of the time series to detect seasonal variability while accounting for scale issues, using the relation, (X(i) − minimum (X))/Range(X), where X indicates monthly average streamflow and precipitation values and *i* denotes the average monthly variable for a particular month. Contour plots of joint probability distributions of severity and duration for **c** meteorological and (d) hydrological droughts for the selected sites. The scatter plots of observed severity and duration (in green circles) are superimposed over the joint CDF contours conforming fit of the copula-based joint distributions. The spacing of contour lines at lower and upper tails show a clear distinction between the selected stations, each belongs to three different climatic regimes. The positive skewness values of drought variables, denoted by γ_1 and γ_2 suggest asymmetry of bivariate drought attributes, severity and duration.

obtained from nonparametric versions of Standardized Runoff Index (N-SRI) and Standardized Precipitation Index (N-SPI) at an accumulation time length (N) of 3- and 6-month, respectively (See Methods and Figure S1 in Supporting Information S1). We then model the nonlinear dependence between drought attributes using copula-based approach (Nelsen, 2013) and subsequently compare multivariate drought hazards associated with milder and extreme droughts based on partial duration series (Brunner et al., 2016) for each study basin. Finally, we analyse the degree of overlap (or imprints) of meteorological versus streamflow droughts across the climate regions using the effect size statistics (Cohen, 1992; see Figure 1).

2. Methods

2.1. Hydrometeorological Forcing Description

To analyze hydrological droughts, we obtain monthly streamflow records archived at the Global Runoff Data Center (GRDC; Grabs, 1997). To choose large river basins (Best, 2018) over the globe, we fix the catchment area as 20,000 km^2 or more as per the criterion of large river basin described in Eisner et al. (2012). To maximize the spatial coverage of large river basins across the globe, we select catchments based on the following criteria (see Figure 2 in Supporting Information S1): (a) Stations with more than 20,000 km^2 catchment area and the mean annual runoff more than 100 m^3/s; and (b) stations with at least 10-month of continuous (free of snowmelts) streamflow records per year and 60 years or more data available. We estimate the missing streamflow records using a time series interpolation technique as adopted earlier in the literature (Ganguli & Ganguly, 2016). (c) To ensure adequate sample lengths to implement a multivariate statistical approach, we consider sites with 40 or more drought events. Overall, these selection criteria yield 278 stream gauges globally covering the period 1806–2017 with varying record lengths depending upon the years of record availability.

To analyze meteorological drought, we use gauge-based monthly gridded precipitation records from the Global Precipitation Climatology Centre (GPCC; Becker et al., 2013) available at a 0.5° spatial resolution. We determine the area-weighted spatial average precipitation over the selected basins considering the influence area of grids by calculating the area of the grid cell located within the catchment weighted by the cosine of the grid latitude (Sheffield & Wood, 2007). For this, we use the delineated watershed boundary available in the GRDC archive for the selected catchments. We maintain the same record lengths retaining area-averaged precipitation and streamflow time-series for each catchment to ensure data compatibility.

2.2. Temporal Evolution of Drought

Typically, the parametric form of distributions, Gamma and Lognormal density functions are often used to fit the SPI (McKee et al., 1993) and SRI (Shukla & Wood, 2008) time series at an aggregated time window of monthly precipitation and streamflow records, respectively. However, the use of a non-parametric form of distribution functions, that is, Gringorten's potting position (rank-based or empirical form) has certain advantages over its parametric form (Hao & AghaKouchak, 2014). The functional form of Gringorten's potting position formula is given below:

$$p(x_i) = \frac{i - 0.44}{n + 0.12} \tag{1}$$

where, n is the sample size, i denotes the rank order statistics of non-zero precipitation aggregated at an n-month (where n = 3 for streamflow droughts and 6 for rainfall-based drought indices) time scales. The advantage of using empirical distributions over parametric distributions is that the former assumes no a priori functional forms and is robust to outliers. Finally, using an equiprobability transformation (McKee et al., 1993), we convert the distribution function of hydro-meteorological time series accumulated at n-month (3- and 6-) time scales into a standardized Gaussian distribution with zero mean and unit standard deviation. We use a non-parametric version of standardized indices to characterize wet/dry/normal states of hydrometeorological time series: SRI considering accumulated runoff of preceding 3 months (SRI3) and SPI considering accumulated rainfall of six preceding months (SPI6) to quantify hydrological and meteorological droughts (Hao & AghaKouchak, 2014) respectively.

While the use of SPI6 is effective in capturing seasonal rainfall deficit and thereby low/high soil moisture status affecting groundwater recharge, which modulates streamflow variability, SRI3 helps in detecting seasonal to short-term streamflow deficits and hence low flow conditions (Shukla & Wood, 2008; Svoboda et al., 2012). In general, streamflow shows higher persistence than precipitation and there is a time lag between peaks of precipitation and streamflow (Dettinger & Diaz, 2000; Özger et al., 2013). Second, the onset of meteorological droughts typically precedes the hydrological droughts. To preserve seasonal variability, we choose different temporal scales in detecting streamflow and precipitation-based droughts. Our approach is based on earlier literature (Huang et al., 2017; Stagge et al., 2018; Wu et al., 2018), in which the authors have shown propagation time from meteorological and streamflow droughts, typically reveals a seasonal characteristics. The spatial map of cross-correlation coefficients using Kendall's τ dependence metric between SRI-3 versus SPI at accumulation lengths, 1, 3, 6, 9, 12, further confirms this finding (See Supplementary figure, Figure S2 in Supporting

Information S1). A significant positive correlation between SPI-*n* and SRI-3 tends to develop for six months of accumulation times across most of the study catchments with a median Kendall's τ value of 0.45 (0.34–0.59 as lower and upper bounds represented by 25th and 75th percentile value of Kendall's τ). Considering 6-month accumulation period, around 20% of gauges show a dependence strength of more than 0.60. Although median spatial Kendall's τ values at higher accumulation periods shows slightly larger values, interestingly, the dependence strength between SPI-*n* and SRI-3 tends to decrease with an increase in accumulation period beyond 6-month, for example, considering 9-month accumulation period, only 5% of gauges show a dependence strength of more than 0.60, whereas, for 12-month accumulation period, only one gauge reports Kendall's $\tau > 0.60$. However, our method is flexible enough to consider either a coherent or different temporal scales for the analysis. We detect drought when monthly values of SRI3 or SPI6 remain below a pre-defined threshold of twentieth percentile (*i.e.*, equaled or exceeded 80% of the time (Svoboda et al., 2012). Drought duration is estimated as the number of consecutive months when SPI6/SRI3 remains below the fixed threshold value and drought severity as the cumulative values of the standardized indices during a drought event.

2.3. Identification of Change Points in Time Series

Often storage, diversions, or other regulation practices affect streamflow time series, impacting hydrological drought trends. To detect possible human influence on multivariate drought attributes, we use non-parametric rank-based Pettitt test (Pettitt, 1979), which is widely used in the literature (Tan & Gan, 2015) for identifying abrupt shifts (i.e., sudden change) in hydro-meteorological time series trends. Figure S3 in Supporting Information S1 presents around 30 stations spatially distributed across all climatic regions show significant (at 5% significant level) change points in the severity and duration time series, which is the consequence of various factors, such as the presence of diversion, dam, reservoir operation and/or land-use changes (Bayazit, 2015). Due to the sparsity of observations in tropics and subtropics, we critically examine the *N*-SRI time series, and their drought attributes series for each station.

We discard the time series before/after for which change points are detected and retain the continuous and uninterrupted part of the SRI time series that exhibit similar variability in the streamflow record with no abrupt shift. Therefore we assume that the effects of changes in the time series are negligible. Further, to maximize the number of gauges, we consider at least 20 or more drought events per site. The use of 20–30 years of record is reasonable for multivariate dependence modeling and is typically in use for hydrologic impact assessment (Mesbahzadeh et al., 2020). The results of the change point test detected a few sites with strong anthropogenic influences in their streamflow drought characteristics even before or after the change point; we did not consider such gauges for further analysis (Table S2 in Supporting Information S1). Finally, we retain 270 stations for the analysis.

2.4. Marginal Distribution Fit of Drought Attributes

Once we estimate drought attributes, severity and duration using the Theory of Runs approach (Sen, 1980) from the standardized indices of precipitation and streamflow time series, we evaluate the marginal distributions of drought attributes using a range of statistical distributions available in the literature (Ganguli & Ganguly, 2016; Rajsekhar et al., 2015). We check the performance of a list of parametric distributions, such as Gamma, Log-normal, Generalized Extreme Value (GEV), and Log-logistic and non-parametric form of distribution, Kernel density estimator to fit drought severity time series. On the other hand, in addition to a list of distributions stated earlier, we also examine the credibility of exponential distribution to fit drought duration time series. We select the best fitted marginal distributions following the minimum AIC criterion (Akaike, 1974). Next, we evaluate the goodness-of-fit tests for the marginal distribution of drought variables using classic bootstrap-based ($N = 500$) Crámer-von-Mises (CvM; integrated squared difference) statistics at a 5% significance level. Following this criterion, ∼93% of gauges pass marginal distribution fit of severity at 5% significance level. On the other hand, ∼ 47–53% gauges qualify marginal distribution fit of duration at a 5% significance level. The gauges which do not satisfies the goodness-of-fit test at desired (*i.e.*, 5% significance level) significance level, we select the most suitable distributions based on the minimum AIC criteria following the literature (Janga Reddy & Ganguli, 2012; Laio et al., 2009).

Tables S3–S6 in Supporting Information S1 summarize the results of marginal distribution fit of bivariate drought properties for meteorological and streamflow droughts, respectively. While for meteorological drought severity,

kernel density estimator fits well for all sites, for hydrological droughts, 93% (252 out of 270) gauges kernel density estimator models the best, followed by the 3% (10 out of 270) share from Lognormal distribution, respectively. The remaining sites are described well by Log logistic, Gamma, and GEV distributions, respectively. For meteorological drought duration, for 60% of sites (162 out of 270), kernel density estimator fits the best, whereas exponential distribution fits the best for the remaining gauges. Likewise, the kernel density estimator models fit the best for 88% sites, followed by the exponential distribution for hydrological drought duration. Figures S4–S5 in Supporting Information S1 show a comparsion of empirical versus theoretical distributions at three representative sites for streamflow droughts. Figure S5 in Supporting Information S1 shows the density and CDF plots of the best-fitted distribution against the histogram of observations and empirical distributions, respectively, which suggest a satisfactory fit between theoretical and empirical distributions.

2.5. Joint Distribution Modeling of Drought Variables

We make use of copulas to model the joint distribution of drought attributes (severity and duration). We evaluate the performance of six different copula families, that is, Clayton (belongs to Archimedean class of copula), Frank (Archimedean class), Gumbel-Hougaard (Both Archimedean and Extreme value class), Negative Logistic Model or Galambos Copula (Extreme value class), Student's t (Elliptical class) and the Rotatory Clayton copulas to link the marginal distributions of mutually dependent drought variables together to form the joint distribution without assuming any specific distributional forms of the marginal (Nelsen, 2013). Out of six different families, the four families, Gumbel-Hougaard, Galambos, Student's t and rotatory Clayton copulas show upper tail behavior. We estimate copula parameters using the maximum pseudo-likelihood (Genest et al., 2009) approach. We assess the goodness-of-fit of the copula-based joint distribution using parametric bootstrap-based ($N = 500$) Cramer von Mises distance statistics at a 5% significance level.

Our analyses show, for all stations, student's t copula fits the best with the highest p-value and the minimum Cramer von Mises distance estimates between empirical and copula-based distribution. Figure S6 in Supporting Information S1 shows the scatter plots of observed drought attributes versus $N = 1000$ random samples from fitted copula families for a representative station, Vicksburg, located at River Mississippi in the subtropical climate regime. Further, the graphical plots of Figure S6 in Supporting Information S1 show the satisfactory performance of the Student's t copula in simulating the complete (as shown by the observed and the simulated Kendall's τ value) versus the upper tail dependence, that is, at the upper right corner of the scatter plot.

2.6. Bivariate Drought Hazard Estimation

We model the joint distribution of drought attributes using the copula function. Since there is no unique definition of the joint return period (JRP) exists, and each definition provides subjective information based on the goal of the study (Serinaldi, 2015), we analyze the bivariate hazard associated with concurrence of drought severity and duration using bivariate return period using "AND" operator, hereafter denoted as JRP_{AND} following Zscheischler and Seneviratne (2017) Here, we consider the JRP_{AND} to compute the joint return period, which is the most extreme scenario in joint probability computation, when both random variables, severity (S) and duration (D), concurrently exceed their reference values (Brunner et al., 2016; Zscheischler & Seneviratne, 2017). It should be noted that the joint return period estimated through "OR" scenario would be a more relaxing in terms of representing the joint return period of the most extreme event; therefore, we do not consider it here. The selected tenth (90th percent exceedance) and 90th (tenth percent exceedance) percentile thresholds for drought attributes constitute milder and extreme drought categories. This provides estimates of the probability of individual hazards exceeding specified (*i.e.*, 10th and 90th percentile) threshold values using the following expression (Brunner et al., 2016)

$$JRP_{AND} = \frac{\zeta}{P(D \geq d \text{ and } S \geq s)} = \frac{\zeta}{1 - F_S(s) - F_D(d) + F_{DS}(d, s)}$$

$$= \frac{\zeta}{1 - u_p - v_p + C_{DS}(u_p, v_p)} \tag{2}$$

where ζ is the average time elapsing between successive drought episodes, u_p and v_p represents sampled extremes exceeding pre-defined thresholds, p = 10th and 90th percentiles for individual drought attributes, that is, $u_p = F_S(s_p)$ and $v_p = F_D(d_p)$.

Assuming drought severity and duration as independent, the term $C_{DS}(u_p, v_p)$ in Equation 2 is replaced by the multiplication of the respective marginal distribution (Singh et al., 2020):

$$JRP_{IND} = \frac{\zeta}{P(D \geq d \text{ and } S \geq s)} = \frac{\zeta}{1 - F_S(s) - F_D(d) + F_{DS}(d, s)} \tag{3}$$

$$= \frac{\zeta}{1 - u_p - v_p + u_p * v_p}$$

The amplification in bivariate drought hazard is computed as the difference between joint return periods under the assumptions of independence versus complete dependence for each catchment, that is, $A = JRP_{IND} - JRP_{AND}$.

Figure S7 in Supporting Information S1 compares the percentage change in multivariate drought hazards under the assumption of independence versus the total dependence considering different copula models for milder and the extreme meteorological (precursor) and hydrological (responder) droughts. While a large variability is apparent for milder hydrological droughts, the meteorological drought exhibit lesser variability. Overall, for milder droughts, the percentage increase in bivariate drought hazard (i.e., underestimation of joint hazard under the assumption of independence) varies between 5%–25% (the left panel in Figure S7 in Supporting Information S1). On the other hand, the percentage amplification in relative risk ranges to the extent of 60%–90% for rare events. Further, it is interesting to note that for rare events, the copulas with upper tail dependence, for example, extreme value class of copulas (Gumbel-Hougaard and Galambos) and the elliptical class of Student's t copula show more substantial amplification in hazard because of its ability to capture the upper tail behavior of extreme events. In all cases, the best performing Student's t copula family shows the most extensive amplification in relative risk implying its ability to capture the low-frequency high impact events due to its fat-tailed behavior.

2.7. Quantification of Effect Size for Multivariate Drought Hazards

We quantify the differences in joint density fields (as indicated by their JRPs) of milder versus extreme categories of droughts through effect size, ε between climate regions. The estimate ε provides extent of overlap between meteorological and hydrological drought hazards considering interdependence between underlying attributes (see Figure 1). For this, we evaluate the signal (change)-to-noise (uncertainty) ratio using the Cohen's D estimate, which measures the differences in mean JRPs between each climate type divided by the pooled standard deviation. Interpretation of Cohen's D is intuitive and enables one to compare two groups even if each group's sample sizes are different. If the variability (expressed by the standard deviation) arises by a chance or noise within the groups, the effect size estimate is nothing but a standardized measure of a signal-to-noise ratio. The general formula of Cohen's D (Cohen, 1992) is as below:

$$D = \frac{M_1 - M_2}{S} \tag{4}$$

where, $S = \sqrt{\frac{(n_1 - 1){S_1}^2 + (n_2 - 1){S_2}^2}{n_1 + n_2 - 2}}$

Here, M_1, S_1 and n_1 are the mean, standard deviation and sample size, of sample Group 1, M_2, S_2 and n_2 are the same for sample Group 2, respectively. S is a measure of standard deviation obtained from the pooled standard deviations of both groups.

However, for the small samples ($n_1 + n_2 \leq 40$), ε is calculated using Hedges' G (Equation 5; Hedges, 1981), a variation of Cohen's D that corrects biases due to sample sizes.

$$J(\nu) = \frac{\Gamma\left(\frac{\nu}{2}\right)}{\sqrt{\frac{\nu}{2}}\Gamma\left(\frac{1}{2}(\nu - 1)\right)} \tag{5}$$

Equation 5 is analytically intractable, hence, the following approximation is proposed in the literature (Hedges, 1981)

$$J(\nu) \approx \left(1 - \frac{3}{4\nu - 1}\right) \tag{6}$$

Finally, Hedges' G is calculated using the following expression (Hedges, 1981)

$$G = J(\nu) \times D \tag{7}$$

Since both of these measures provide a single estimate of overall uncertainty (signal-to-noise ratio), we estimate statistical uncertainty around ϵ using 1000 random runs of effect size statistics through a bootstrap-based resampling technique. Finally, we report the *most likely* (50th percentile value), statistical significance of the estimates at a 5% significance level and corresponding confidence bounds.

Following earlier studies (Cohen, 1992) and more recently in Gevaert et al. (2018), we use the values of $0.2 < \varepsilon < 0.5$, $0.5 < \varepsilon < 0.8$, $0.8 < \varepsilon < 1.7$, and ≥ 1.7 to interpret small, medium, large, and very large effect sizes, respectively. An effect size value of 0 indicates distributions of drought categories across a climate regime completely overlaps each other. A small effect size between drought types shows strong multivariate drought overlap between meteorological and hydrological droughts. In contrast, an effect size of 1.7 indicates a non-overlap of ~75.4% in the two distributions with a substantial variation in multivariate drought hazard between two drought groups (Becker, 2000), indicating weaker imprints. Accordingly, an effect size of 0.5 infers a magnitude equivalent to a one-half standard deviation change between two drought categories. While a previous study (Van Loon et al., 2014) is limited to quantifying differences in bivariate density fields among disparate climate regions by the slope of linear regression lines, our approach offers quantifying the strength of the relationship between two nonlinear distributions through the effect size statistics, which accounts for the dissimilar length of samples within groups. Further, we report the uncertainty associated with the effect size statistics and corresponding 95% confidence interval through a bootstrap-based resampling.

3. Results

3.1. Stronger Dependence of Hydrological Drought Attributes Relative to Meteorological Drought

Since univariate modeling of drought attributes may lead to over/underestimation of drought hazards (AghaKouchak et al., 2014; Zscheischler & Seneviratne, 2017), we model bivariate drought hazards across different river basins within three climate types. First, we analyze the dependence between drought attributes, severity and duration using a non-parametric Kendall's correlation coefficient (or Kendall's τ; see Methods). We start our analysis by showing the exemplary plots of precipitation and streamflow regimes for three selected catchments in different climate regions, along with their respective (copulas-based) dependency structures for hydrological and meteorological droughts (Figures 2b–2d). The time series of monthly flow patterns and precipitation at selected gauging stations across climate regions suggest a distinct hydroclimatic pattern; for instance, River Rio (Figure 2b; top panel) displays a moderate peak discharge around mid-autumn, which is a typical flow regime observed in a tropical river basins (Haines et al., 1988). Likewise, River Danube (Figure 2b; bottom panel) displays no distinct low flow episode with autumn peaks likely to be absent, which is a characteristic of *moderate-spring* discharge regime (Haines et al., 1988). Furthermore, the scatterplots of bivariate drought attributes, superimposed over the joint probability distribution of meteorological (Figure 2c) and hydrological droughts (Figure 2d), reflect the impact of climate types on multivariate drought imprints. The positive skewness of drought attributes (Figures 2c and 2d) indicates the asymmetric behavior of drought variables with a long right tail. Further, except for meteorological drought severity in the Danube catchment (Figure 2c), kurtosis of drought attributes is greater than 3, indicating heavy-tailed behavior. The asymmetric and heavier tail behavior of drought attributes necessitates copulas to model bivariate drought hazards. The contour lines in a tropical river basin are closely spaced at lower probability levels, indicating sharp gradient changes as compared to river basins in other two climate types, while the opposite trend is apparent at higher probability levels. We find a distinct pattern in the contour lines near the tail ends, reflecting a difference in probability values at upper and lower quantiles of joint distributions across the climate types, which a simple linear relationship fails to simulate.

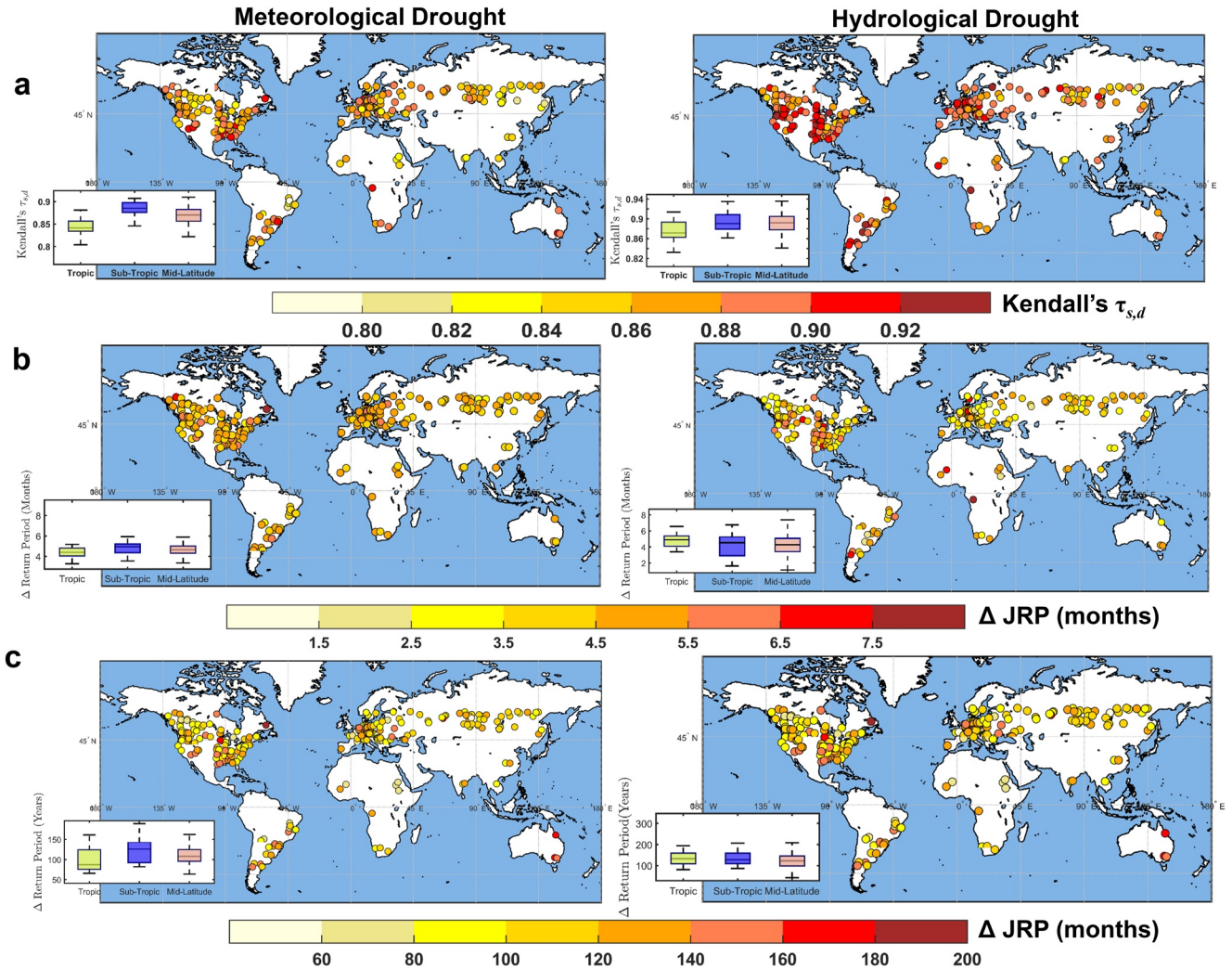

Figure 3. Spatial variations in dependence strengths and difference in bivariate drought hazards for milder and extreme categories of meteorological (left panel) versus hydrological (right panel) droughts for climate regions. (a) Dependence between drought attributes, severity and duration is estimated using nonparametric dependence metric Kendall's τ. The difference in bivariate drought hazards, joint return periods (ΔJRP) considering with and without dependence for (b) milder (tenth percentile exceedance probability of drought attributes) and (c) extreme (90th percentile exceedance probability of drought attributes) droughts. The boxplots in the inset show distribution of dependence and differences in drought hazards considering with and without dependence of univariate statistics. Box center marks (black lines) are medians; box bottom and top edges show 25th and 75th percentiles respectively, whereas the spread of the boxes indicates interquartile range; whiskers indicate $q_{75} + 1.5(q_{75} - q_{25})$ and $q_{25} - 1.5(q_{75} - q_{25})$, where q is the quantiles of variables.

Across all analyzed catchments, we find a significant (at p-value < 0.05) strong correlation (>0.70) between severity and duration for both meteorological (SPI6) and hydrological (SRI3) droughts (Figure 3a). However, while only ~5% (14 out of 270) catchments show Kendall's τ value more than 0.90 for meteorological drought (Figure 3a, *left panel*), over 30% (89 out of 270) catchments show a strong Kendall's τ value of ≥0.9 for hydrological droughts (Figure 3a, *right panel*). Among three climate types, subtropics show the strongest dependence as demonstrated by a strong dependence pattern with a median value of Kendall's τ greater than 0.88 for rain-deficit and streamflow-based droughts. Despite the Millennium drought (~2001–2009) in southeast Australia (Van Dijk et al., 2013), the strength of correlations over Australian catchments are in the order of 0.89 for Southern Australia. The La Plata River basin in South America is one of the largest river basins in the world, includes many sub-basins like Paraná and Uruguay, show a stronger dependence in both meteorological (ranges from 0.87 to 0.90) and hydrological droughts (Kendall's τ value ranges from 0.86 to 0.93). The Yangtze River basin in China shows a higher dependence in case of hydrological drought (Kendall's τ value ranges between 0.88 and 0.90 for GRDC gauge ID 2181600 and 2181800) compared to meteorological drought (Kendall's τ value of in the range of 0.84–0.85). On the other hand, river basins across the tropics show lower dependence strength than

the other two climate types. For example, the gauges across tropical monsoon climate regions, India's Godavari and Krishna river basins show relatively low dependence with Kendall's τ value of 0.83–0.84 for both meteorological and hydrological droughts. In South Asia, seasonality dominates drought propagation, where the timing of precipitation has a significant impact (Apurv et al., 2017; Van Loon, 2015). In Africa, the River Congo shows a relatively higher dependence value with Kendall's τ value ranges between 0.92 and 0.94 respectively for meteorological and hydrological droughts. Overall, in tropics, the dependence value for streamflow-based drought ranges from 0.86 to 0.89 (the 25th and 75th percentile bounds) with a median value 0.87 (Figure 3a, *right panel*). In contrast, the dependence value for the meteorological drought is comparatively low and ranges between 0.83 and 0.86 with a median value of 0.84 (Figure 3a, *left panel*). Likewise, basins located in mid-latitudes show a similar trend, that is, an apparent higher dependence in hydrological droughts with a median Kendall's τ value of 0.89 (0.88–0.90 as an interquartile range) as compared to the meteorological drought with a median Kendall's τ value of 0.87 (0.86–0.88). Over (mid-latitudes) in Central Europe, extreme droughts have been linked with an increase in temperature and record-breaking heatwaves since the 2000s, compounded by a lack of precipitation during summer months (Hanel et al., 2018; Hari et al., 2020).

Overall, the spatial map of Kendall's τ suggests a stronger dependence of drought attributes in hydrological droughts than that of the meteorological droughts in all climatic regions over the globe. The observed high correlation between drought attributes further confirms the need for multivariate modeling (severity vs. duration) for a systematic evolution of catchment-scale drought propagation. On the other hand, dependence between underlying attributes was not considered in earlier assessments (Gevaert et al., 2018; Van Loon et al., 2014) to explain the catchment-scale propagation of drought dynamics over different climate types.

3.2. Contrasting Response of Milder Versus Extreme Drought Hazards

To further examine how the nature of dependence evolves under different drought categories (i.e., milder and extreme droughts) and climate types, we compare the difference in joint return periods (JRP) considering perfect dependence (JRP_{AND}) versus independence (JRP_{IND}) across individual stream gauges (See Methods for the JRP details). We contrast these differences for the milder and extreme droughts for the 90th percent and tenth percent exceedance probability of drought attributes, that is, severity and duration (see Methods). It is worth noting that since the available record lengths are different across sites (Figure 2) and we compute bivariate drought hazards of extreme drought attributes, the calculated joint return periods are not uniform across the sites, indicating the joint exceedance probability varies across catchments and climate types over the globe. The difference in JRPs tends to get larger for extremes (≥100-year) for 65%–76% spatial locations, whereas for milder droughts, differences are minor, often less than six months (Figures 3b and 3c) for more than 90% of sites. In addition, for meteorological drought, the difference in joint return period is relatively higher in subtropics as compared to the other two climate types, which could be because of stronger dependence between drought attributes in this region (Zscheischler & Seneviratne, 2017).

For extreme droughts, the difference between JRP_{AND} and JRP_{IND} tends to get larger–the site with stronger dependence shows a more significant difference in JRPs (Figures 3a and 3c). For example, in extreme hydrological droughts, the difference in joint return periods ranges from 52 to >100 years for the sites with Kendall's τ greater than 0.90. The role of dependence in JRP_{AND} is the strongest that shows considerably smaller return periods or frequent occurrence of drought events than that of the joint return period computed under the assumption of independence. The question arises as to how sensitive is the difference in estimated joint return periods (*i.e.*, complete dependence vs. the assumption of independence) at high values of complete dependence (obtained from Kendall's τ) for milder and extreme categories of droughts. The difference in joint return periods (*JRPs*) versus Kendall's τ shows a distinct power-law relationship (Figure 4). For instance, the amplification (A) in joint return periods increase with Kendall's τ that has implications for probabilistic hazard estimates of rare events (Zscheischler & Seneviratne, 2017). We derive the following relationship for the power-law growth (Figure 4) of the bivariate drought hazard relating the difference in joint return periods (*i.e.*, JRP_{IND}–JRP_{AND}) versus the robust dependence metric (Kendall's τ; Yang et al., 2020) given as

$$A = \alpha\tau^{\lambda}, \lambda > 0, \tau > \tau_{min} \quad (8)$$

A is amplifications in bivariate drought hazard considering without versus with inter-dependence between drought attributes. Where α and λ are constants; here λ indicates growth exponent. A value of $\lambda > 1$ indicates

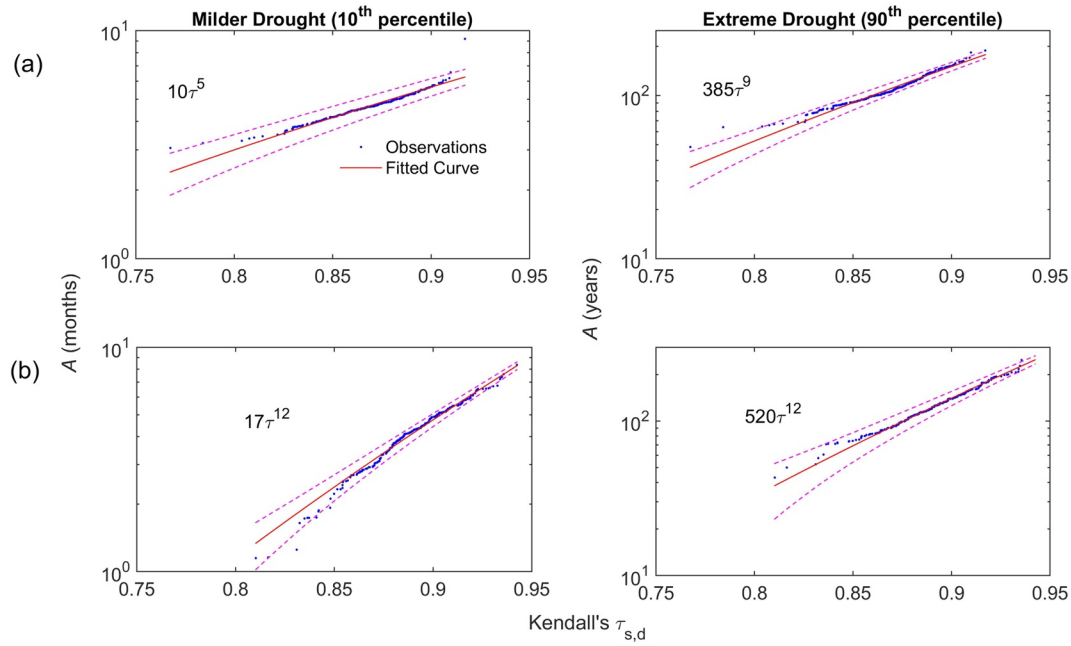

Figure 4. Amplifications in drought hazard with growth exponent $\lambda > 1$. Scatter plots showing amplifications in return periods $A = \mathrm{JRP}_{IND} - \mathrm{JRP}_{AND}$ versus the nonparametric dependence metrics Kendall's τ for (a) Meteorological droughts (b) Hydrological droughts. The solid line in blue is the least-square fitting in a semi-logarithmic plot with R^2 values ranging from 0.90–0.99. Vertical (Y)-axes are on logarithmic scale, where *log* (.) is the natural logarithm. The uncertainty envelops (dotted lines in magenta) shows the 95% confidence interval associated with the power-law fit.

that the difference in joint return periods amplifies with an increase in dependence between underlying drought drivers. The presence of power-law tails leads to a much larger number of extremes than it would have been possible by assuming independence between drought attributes. The slope of the least-square fitting corresponds to λ and the starting point of the linear fitting is $\tau_{\mathrm{min.}}$ The amplification in drought hazard versus Kendall's τ satisfies power-law behavior with $\lambda = 5$ (within lower and upper bounds 5.16–5.6)–9 (within 8.7–9.1) for milder and extreme categories of meteorological droughts, whereas $\lambda = 12$ (within 11.9–12.2 for milder and within 12.16–12.7 for extreme categories) for hydrological droughts, respectively. Interestingly, the growth exponent λ for hydrological droughts are larger as compared to the meteorological drought. A stronger dependency between drought attributes in hydrological drought (Figure 3a) than that of the meteorological drought resulted in large value of the power-law exponent (λ). The detection of a power-law growth of the bivariate drought hazards indicates extremes tend to be more severe and frequent than would otherwise be expected if independent or a combination of univariate distributions are assumed (Zscheischler et al., 2020).

3.3. Multivariate Drought Imprints Among Different Climate Regions

Next, we analyze the multivariate imprints of meteorological to hydrological droughts across climate types and drought categories (milder vs. extreme) in pursuit of underpinning the role of preconditioning drivers (meteorological droughts) on the responder (streamflow droughts). To compare inter-regional variations in hydrological versus meteorological drought hazard footprints, we use the effect size statistic (Cohen, 1992) that compares the difference between group means and its variability by standardizing the effect magnitude. The standardization is performed in the effect size statistics so that the calculated statistics are compatible across all climate types. We compute ε using Cohen's D for large samples ($n_1 + n_2 > 40$, where n_1 and n_2 are the sample sizes of individual groups, See Methods). However, in regions with fewer sites, we use Hedges' G (e.g., Tropics) to estimate ε, a variation of Cohen's D that corrects biases due to the small sample sizes (see Methods for details).

Figure 5 compares the distribution of bivariate drought hazard of meteorological versus hydrological droughts for milder (Figure 5 top panel) versus extreme (Figure 5 bottom panel) droughts. The tabulated values in Figure 5 show the inter-regional imprints of extreme droughts using effect size statistics. We determine the uncertainty

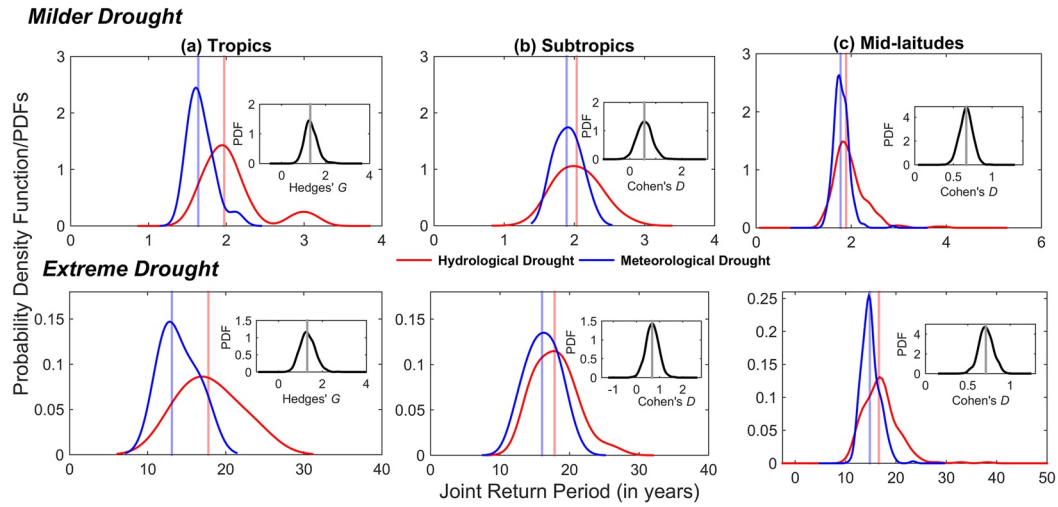

Meteorological to Hydrological	Median Effect Size Statistics	Lower Bound	Upper Bound	*p*-value (Effect Size)	*p*-value (KS test)
Milder (10th Percentile)					
Tropics	1.24 (1.30)	0.77	1.96	0.001**	0.003**
Subtropics	0.55 (0.56)	0.04	1.20	0.02**	0.07*
Mid-latitudes	0.66 (0.66)	0.51	0.84	0.001**	< 0.001**
Extreme (90th Percentile)					
Tropics	1.28 (1.29)	0.68	2.10	0.001**	0.03**
Subtropics	0.67 (0.68)	0.14	1.23	0.006**	0.26
Mid-latitudes	0.71 (0.71)	0.55	0.89	0.001**	< 0.001**

Figure 5. Multivariate overlaps of meteorological to hydrological droughts for milder and rare events across climate types. The density functions (upper and middle panel) of bivariate drought hazards compares the meteorological (blue) and hydrological droughts (in red). Inset shows the PDFs (in gray) of effect size statistics indicating the extent of overlap obtained from 1000 bootstrap samples. The table below compares JRP_{AND} estimates of the effect size statistics and their 95% confidence intervals. Values in the parentheses show the "*most likely*" effect size statistics obtained from the median (50th percentile) estimates of bootstrap resamples. The last but one column shows the p-value associated with the effect size statistics, whereas the last column indicates the p-value obtained from testing the difference in two distributions. The single ("*") and double ("**") asterisks indicate statistical significance at 5% and 1% significance levels.

in effect size statistics from $N = 1000$ random bootstrap runs (see the *most likely* scenario and the upper and lower bounds, *i.e.,* the 50th percentile value with 95% confidence intervals, and p-values in Figure 5 as tabulated values). Except for subtropics, the other two regions show a clear significant shift in density functions of meteorological versus hydrological droughts for both milder and extreme droughts as confirmed by the two-sample Kolmogorov-Smirnov test (p-value < 0.05; see the tabulated list in Figure 5). In contrast, Subtropics show considerable overlaps between two PDFs with a *p*-value > 0.05, indicating it fails to reject the null hypothesis that the two distributions (*i.e.*, meteorological vs. hydrological) are significantly different at a 5% significance level. A quantitative comparison of bivariate hazard imprints (or degree of overlap) of hydrological versus meteorological drought shows a medium positive effect (in the order of 0.5 or slightly higher than that) for subtropics and mid-latitudes regions. However, bivariate hazard imprints in the tropics exceed 1-standard deviation, indicating weaker imprints or little overlap of meteorological versus streamflow droughts. The detected effect size statistics are robust (i.e., p-value < 0.05) across all regions.

The positive effect sizes of multivariate drought hazard between hydrological and meteorological droughts in all climate types suggest higher JRPs of hydrological droughts than those of meteorological. This also implies meteorological droughts, owing to their less persistency than streamflow droughts, show shorter mean recurrence time between two consecutive episodes, resulting in more frequent events with lower JRPs than hydrological ones

in all climates. The propagation of droughts through the hydrological cycle owing to the pooling and lengthening of prolonged meteorological droughts results in persistent long-duration streamflow droughts (Van Loon, 2015).

In particular, in the tropics, the density functions of JRP_{AND} (Figure 5; *top and the middle panels*) show somewhat different behavior than that of the other two climate types together with a "large" effect size (Hedges'G) for both categories droughts (milder and extreme). There is a distinct translation pattern from meteorological JRP_{AND} to hydrological JRP_{AND} in their density diagrams. A notable shift in PDFs of hydrological drought is apparent, accompanied by a substantial variability as reflected from a relatively flatter shape of PDFs in hydrological droughts compared to the meteorological droughts with a large return period. The shift in the variability of density function indicates precipitation deficits in the short term have fewer linkages with streamflow, but the long-term deficits have a more robust response to streamflow. This informs the complex propagation of droughts in the tropics due to local catchment characteristics and underlying terrestrial hydrological processes (Grayson & Blöschl, 2001; Tallaksen & Van Lanen, 2004). On the other hand, the mid-latitude climate regime shows a little higher value than the medium effect size (Figure 5, *bottom panel*), suggesting the presence of less frequent but longer duration, persistent hydrological droughts in this region. Our findings corroborate previous studies (Gibson et al., 2019; Naranjo et al., 2018; Roundy et al., 2012; Van Loon, 2015), which show precipitation deficit does not necessarily translate into hydrological droughts; land-atmospheric feedbacks, climate, and catchment control play a vital role in propagating droughts. Further, in mid-latitudes, a combination of successive dry winter/spring seasons and prolonged soil moisture deficit followed by a lack of groundwater recharge can cause persistent hydrological droughts in slow responding catchments during summer (Hanel et al., 2018; Marsh et al., 2007; Van Loon, 2015). Over north-western Europe, multi-year hydrological droughts with extended spatial coverage have often been linked to recurrent dry winter episode (Kendon et al., 2013; Parry et al., 2012).

In contrast, the subtropics, which lies in a transitional climate regime, the multivariate JRP_{AND} of meteorological versus hydrological drought, overlaps with each other in the extreme case (Figure 5). In contrast, a little shift is observed in milder cases, accompanied by a change in the variability of the density function for hydrological drought. A visual inspection of PDFs corresponding to the meteorological versus hydrological drought hazard for subtropics shows a relatively symmetric shape of the distributions compared to the PDFs of the other two regions. A near symmetric distribution indicates lesser variability in the distribution of extremes in this region. The subtropical climate regime shows small to medium effect sizes between hydrological and meteorological droughts, with values ranging from 0.04 to 1.23 (considering 95% confidence bounds). The effect size statistics in subtropics are smaller than in the other two regions, which indicates strong multivariate imprints between meteorological and streamflow droughts. The presence of strong coupling between soil moisture and precipitation has been reported previously (Koster et al., 2004; Wei et al., 2016) for this region, which possibly dictate a relatively stronger imprints of meteorological (preconditioning driver) to hydrological (response) droughts.

4. Discussion

Drought and water stress pose a significant challenge in global water security in a warming climate (Raymond et al., 2020; Zscheischler et al., 2018). Using gauge-based observational records of 270 catchments, we present a global synthesis of multivariate aspects of different drought types and show the role of climate and the dependence structure impacting joint exceedance of drought attributes. While meteorological droughts act as a (preconditioning) causal driver for hydrological droughts (a responder), the presence of nonlinear dependence between the underlying attributes may affect the translation pattern of meteorological to hydrologic droughts. Our findings corroborate with a growing body of the literature (AghaKouchak et al., 2014a; Hao & AghaKouchak, 2014; Zscheischler & Seneviratne, 2017) that highlighted the importance of considering nonlinear dependence between underlying drought attributes in assessing multivariate drought hazards, failure of which may lead to over/under-estimation of hazard/risk. We demonstrate the contrasting differences in the bivariate hazards of milder versus extreme categories of droughts in space and time at a global scale using observational precipitation and streamflow records.

Considering extreme droughts, we identify more than 100 years of differences in bivariate drought hazards across sites, accounting for dependence between drought attributes compared to joint return periods with assumptions of independence. Further, we establish a power-law relation of the amplifications in bivariate drought hazard-to-dependence, which implies extremes tend to be more severe and frequent than would otherwise be expected if

drought attributes were independent or linearly dependent. Based on the bivariate drought hazard and effect size metric, we further show distinct responses in multivariate hazard imprints across climate types with little changes in precipitation-deficit versus streamflow droughts across subtropics, indicating substantial overlaps between drought types for this region. In contrast, a large effect size in the tropics indicates substantial variations in meteorological versus hydrological droughts suggesting weaker imprints (small overlaps) between drought types. Our findings are in agreement with the literature that showed that the propagation of droughts in the tropics follows a complex pattern (Van Loon et al., 2014), whereas, in subtropics, a quicker response is apparent from meteorological to hydrological droughts (Gevaert et al., 2018). Subtropical catchments have a relatively stable climate type, such as temperature and precipitation show relatively fewer fluctuations across the year with no sub-zero temperature and without pronounced seasonal influence (e.g., monsoon) or slowly varying rainfall cycle (Naranjo et al., 2018; Van Loon et al., 2014). This further suggests that catchment characteristics have a relatively lesser role in drought propagation in subtropical catchments than those in the other two climate regimes. While several large-scale assessments are often confined to either virtual catchments (Apurv et al., 2017; Van Loon et al., 2014) or utilizing stochastically simulated streamflow records (Brunner & Tallaksen, 2019), using gauge-based observational records in a multivariate framework, here we, however, identified several hotspots that are not well documented in the literature. Frequent and severe droughts are observed for catchments across northern Australia, Eastern Europe (sites across Ukraine and neighboring countries), and a few regions of the south-eastern United States and eastern Canada (Figure 3c), indicating these regions require greater attention to inform extreme droughts.

A few caveats of the current analysis are worth noting. While our hydrological and meteorological drought analyses are solely based on gauge-based records, spatiotemporal coverage of observations remains a limiting factor. For instance, the specific insights depend on the quality of streamflow records in regions with sparse data coverage (such as south Asia and Africa). Use of alternate sources of data records, either gauged-based (Gudmundsson et al., 2018), re-analysis (Harrigan et al., 2020), and/or high-resolution gridded hydrometric reconstructions (Ghiggi et al., 2019) may improve confidence; however, at the cost of inherent limitations; for example, model structural/parameterization uncertainties in reconstructed datasets. In a bivariate framework, the uncertainty may stem from limited sample lengths, and distribution fitting, such as uncertainty related to marginal distribution together with the uncertainty associated with dependence structure of two variables (Brunner et al., 2016). Despite we use the long time series of quality-controlled observational records, considering different sources of uncertainty in bivariate framework, we assume that the effects of changes in the time series are not large. Although in tropics and sub-tropics, the effect of snow melts in drought propagation would be negligible over the selected sites, over mid-latitudes shift in snowmelt timing and below-average snowpack (snow drought) could result in below-normal summer streamflow and streamflow droughts (Huning & AghaKouchak, 2020; Winchell et al., 2016). In our analyses, we have not considered the effect of snow melts and its variations on catchment-scale hydrologic drought responses as our analysis focused more on an integrated aspect of streamflow drought, resulting from precipitation variability. We encourage future studies to further disentangle and specify the varying role of different hydrological processes (e.g., snow, soil-moisture, evapotranspiration) in a multivariate settings of drought propagation. While a detailed process-based investigation of catchment-scale drought propagation is beyond the scope of the current study, we emphasize that our copula-based approach provides a statistical exploration and establish linkages between multivariate drought hazards, considering overlaps or imprints of one drought type (meteorological) to another (hydrological) across different climate regions. Further, we present associated uncertainty through a standardized measure of a signal-to-noise ratio. While a higher accumulation length in the precipitation index, compared to the runoff one, adopted in this study to some degree reflects internal catchment functioning of dampening process, we encourage future studies to jointly investigate the dependence structure through (process-based) modeling and statistical techniques while carefully accounting for inherent uncertainties (e.g., in model parametrizations or statistical quantifications).

Nevertheless, the obtained results of robust amplifications in bivariate drought hazards provide a systematic view on observation-based drought imprints across different climatic regions over the globe. This can serve as a potential benchmark for stakeholders in formulating drought adaptive strategies across the world's large River basins, and developing risk-informed decisions for the resilience of critical infrastructure. Further, the derived insights will aid in forecasting efforts and evaluating the performance of hydrological and land-surface models to address impact-relevant case-studies (Krysanova et al., 2020; Wanders et al., 2019). Our analyses reveal a strong amplification in multivariate drought hazards accounting dependence, especially for extreme droughts, which has

implications for "safe" design of water resources systems, such as regulation and planning of water reservoirs and adaptation to extreme droughts (Wan et al., 2017). Overall, our results highlight the importance of considering drought propagations in a multivariate lens, which helps to identify hotspots of climate-mediated change in drought dynamics across river basins around the globe (Falkenmark et al., 2019).

Conflict of Interest

The authors declare no conflicts of interest relevant to this study.

Data Availability Statement

The station-based streamflow time series are downloaded from the GRDC data centre (https://portal.grdc.bafg.de/applications/public.html?publicuser=PublicUser). The gridded time series of precipitation is obtained from the GPCC (https://opendata.dwd.de/climate_environment/GPCC/html/download_gate.html) archive.

Acknowledgments
PG is supported through Science and Engineering Research Board, Government of India's early career start-up grant, SRG/2019/000044. The Indian Institute of Technology Kharagpur provided partial funding through the Institute Seed grant. AM was supported through DAAD fellowship of Combined Study and Practice Stays for Engineers from Developing Countries (KOSPIE) with Indian IITs, 2019 (Funding ID 57503493), for 7 months graduate program at Technical University of Dresden, Germany. Open Access funding enabled and organized by Projekt DEAL.

References

AghaKouchak, A., Cheng, L., Mazdiyasni, O., & Farahmand, A. (2014). Global warming and changes in risk of concurrent climate extremes: Insights from the 2014 California Drought. *Geophysical Research Letters*, *41*(24), 8847–8852. https://doi.org/10.1002/2014gl062308

Akaike, H. (1974). A new look at the statistical model identification. *IEEE Transactions on Automatic Control*, *19*(6), 716–723. https://doi.org/10.1109/tac.1974.1100705

Apurv, T., Sivapalan, M., & Cai, X. (2017). Understanding the role of climate characteristics in drought propagation. *Water Resources Research*, *53*(11), 9304–9329. https://doi.org/10.1002/2017wr021445

Bayazit, M. (2015). Nonstationarity of hydrological records and recent trends in trend analysis: A state-of-the-art review. *Environmental Processes*, *2*(3), 527–542. https://doi.org/10.1007/s40710-015-0081-7

Becker, A., Finger, P., Meyer-Christoffer, A., Rudolf, B., Schamm, K., Schneider, U., & Ziese, M. (2013). A description of the global land-surface precipitation data products of the Global Precipitation Climatology Centre with sample applications including centennial (trend) analysis from 1901–present. *Earth System Science Data*, *5*(1), 71–99. https://doi.org/10.5194/essd-5-71-2013

Becker, L. (2000). Effect size (ES). Retrieved from https://www.uv.es/~friasnav/EffectSizeBecker.pdf

Best, J. (2018). Anthropogenic stresses on the world's big rivers. *Nature Geoscience*, *12*(1), 7–21. https://doi.org/10.1038/s41561-018-0262-x

Brunner, M. I., Seibert, J., & Favre, A.-C. (2016). Bivariate return periods and their importance for flood peak and volume estimation: Bivariate return periods. *Wiley Interdisciplinary Reviews: Water*, *3*(6), 819–833. https://doi.org/10.1002/wat2.1173

Brunner, M. I., & Tallaksen, L. M. (2019). Proneness of European catchments to multiyear streamflow droughts. *Water Resources Research*, *55*(11), 8881–8894. https://doi.org/10.1029/2019wr025903

Chang, J., Li, Y., Wang, Y., & Yuan, M. (2016). Copula-based drought risk assessment combined with an integrated index in the Wei River Basin, China. *Journal of Hydrology*, *540*, 824–834. https://doi.org/10.1016/j.jhydrol.2016.06.064

Cheng, L., Hoerling, M., AghaKouchak, A., Livneh, B., Quan, X.-W., & Eischeid, J. (2015). How has human-induced climate change affected California Drought risk? *Journal of Climate*, *29*(1), 111–120. https://doi.org/10.1175/jcli-d-15-0260.1

Clark, M. P., McMillan, H. K., Collins, D. B., Kavetski, D., & Woods, R. A. (2011). Hydrological field data from a modeller's perspective: Part 2: Process-Based evaluation of model hypotheses. *Hydrological Processes*, *25*(4), 523–543. https://doi.org/10.1002/hyp.7902

Clark, M. P., Slater, A. G., Rupp, D. E., Woods, R. A., Vrugt, J. A., Gupta, H. V., et al. (2008). Framework for understanding structural errors (FUSE): A modular framework to diagnose differences between hydrological models. *Water Resources Research*, *44*(12). https://doi.org/10.1029/2007wr006735

Cohen, J. (1992). A power primer. *Psychological Bulletin*, *112*(1), 155–159. https://doi.org/10.1037/0033-2909.112.1.155

Dankers, R., & Feyen, L. (2009). Flood hazard in Europe in an ensemble of regional climate scenarios. *Journal of Geophysical Research*, *114*(D16), D16108. https://doi.org/10.1029/2008JD011523

Das, J., Jha, S., & Goyal, M. K. (2020). Non-stationary and copula-based approach to assess the drought characteristics encompassing climate indices over the Himalayan states in India. *Journal of Hydrology*, *580*, 124356. https://doi.org/10.1016/j.jhydrol.2019.124356

Dettinger, M. D., & Diaz, H. F. (2000). Global characteristics of stream flow seasonality and variability. *Journal of Hydrometeorology*, *1*(4), 289–310. https://doi.org/10.1175/1525-7541(2000)001<0289:gcosfs>2.0.co;2

Dixit, S., & Jayakumar, K. V. (2021). A study on copula-based bivariate and trivariate drought assessment in Godavari River basin and the teleconnection of drought with large-scale climate indices. *Theoretical and Applied Climatology*, *146*(3), 1335–1353. https://doi.org/10.1007/s00704-021-03792-w

Eisner, S., Voss, F., & Kynast, E. (2012). Statistical bias correction of global climate projections–consequences for large scale modeling of flood flows. *Advances in Geosciences*, *31*, 75–82. https://doi.org/10.5194/adgeo-31-75-2012

Falkenmark, M., Wang-Erlandsson, L., & Rockström, J. (2019). Understanding of water resilience in the Anthropocene. *Journal of Hydrology X*, *2*, 100009. https://doi.org/10.1016/j.hydroa.2018.100009

FAO (Food and Agriculture Organization of the United Nations). (2018). *Disasters causing billions in agricultural losses, with drought leading the way*. FAO. Retrieved from https://www.fao.org/news/story/en/item/1106977/icode/

Ganguli, P., & Ganguly, A. R. (2016). Space-time trends in U.S. meteorological droughts. *Journal of Hydrology: Regional Studies*, *8*, 235–259. https://doi.org/10.1016/j.ejrh.2016.09.004

Genest, C., Rémillard, B., & Beaudoin, D. (2009). Goodness-of-fit tests for copulas: A review and a power study. *Insurance: Mathematics and Economics*, *44*(2), 199–213. https://doi.org/10.1016/j.insmatheco.2007.10.005

Gevaert, A., Veldkamp, T., & Ward, P. (2018). The effect of climate type on timescales of drought propagation in an ensemble of global hydrological models. *Hydrology and Earth System Sciences*, *22*(9), 4649–4665. https://doi.org/10.5194/hess-22-4649-2018

Ghiggi, G., Humphrey, V., Seneviratne, S. I., & Gudmundsson, L. (2019). GRUN: An observation-based global gridded runoff dataset from 1902 to 2014. *Earth System Science Data*, *11*(4), 1655–1674. https://doi.org/10.5194/essd-11-1655-2019

Gibson, A. J., Verdon-Kidd, D. C., Hancock, G. R., & Willgoose, G. (2019). Catchment-scale drought: Capturing the whole drought cycle using multiple indicators. *Hydrology and Earth System Sciences Discussions*, *24*(4), 1–33. https://doi.org/10.5194/hess-24-1985-2020

Grabs, W. (1997). Report on the third meeting of the GRDC Steering Committee. *Technical Reports Series*. Retrieved from https://www.bafg.de/GRDC/EN/02_srvcs/24_rprtsrs/reports_node.html

Grayson, R., & Blöschl, G. (2001). *Spatial patterns in catchment hydrology: Observations and modelling*. Cambridge University Press.

Greve, P., Gudmundsson, L., & Seneviratne, S. I. (2018). Regional scaling of annual mean precipitation and water availability with global temperature change. *Earth System Dynamics*, *9*(1), 227–240. https://doi.org/10.5194/esd-9-227-2018

Gu, L., Chen, J., Yin, J., Xu, C.-Y., & Chen, H. (2020). Drought hazard transferability from meteorological to hydrological propagation. *Journal of Hydrology*, *585*, 124761. https://doi.org/10.1016/j.jhydrol.2020.124761

Gu, L., Chen, J., Yin, J., Xu, C.-Y., & Zhou, J. (2020). Responses of precipitation and runoff to climate warming and implications for future drought changes in China. *Earth's Future*, *8*(10), e2020EF001718. https://doi.org/10.1029/2020ef001718

Gudmundsson, L., Do, H. X., Leonard, M., & Westra, S. (2018). The global streamflow indices and metadata archive (GSIM)—Part 2: Quality control, time-series indices and homogeneity assessment. *Earth System Science Data*, *10*(2), 787–804. https://doi.org/10.5194/essd-10-787-2018

Guha-Sapir, D., Hoyois, P., Wallemacq, P., & Below, R. (2017). *Annual disaster statistical review 2016: The numbers and trends* (pp. 1–80). Brussels, Belgium: Centre for Research on the Epidemiology of Disasters (CRED). Retrieved from https://reliefweb.int/sites/reliefweb.int/files/resources/adsr_2016.pdf

Haines, A. T., Finlayson, B. L., & McMahon, T. A. (1988). A global classification of river regimes. *Applied Geography*, *8*(4), 255–272. https://doi.org/10.1016/0143-6228(88)90035-5

Hanel, M., Rakovec, O., Markonis, Y., Máca, P., Samaniego, L., Kyselý, J., & Kumar, R. (2018). Revisiting the recent European droughts from a long-term perspective. *Scientific Reports*, *8*(1), 1–11. https://doi.org/10.1038/s41598-018-27464-4

Hao, Z., & AghaKouchak, A. (2014). A nonparametric multivariate multi-index drought monitoring framework. *Journal of Hydrometeorology*, *15*(1), 89–101. https://doi.org/10.1175/jhm-d-12-0160.1

Hao, Z., & Singh, V. P. (2015). Drought characterization from a multivariate perspective: A review. *Journal of Hydrology*, *527*, 668–678. https://doi.org/10.1016/j.jhydrol.2015.05.031

Hari, V., Rakovec, O., Markonis, Y., Hanel, M., & Kumar, R. (2020). Increased future occurrences of the exceptional 2018–2019 Central European drought under global warming. *Scientific Reports*, *10*(1), 1–10. https://doi.org/10.1038/s41598-020-68872-9

Harrigan, S., Zsoter, E., Alfieri, L., Prudhomme, C., Salamon, P., Wetterhall, F., et al. (2020). GloFAS-ERA5 operational global river discharge reanalysis 1979-present. *Earth System Science Data*, *12*(3), 2043–2060. https://doi.org/10.5194/essd-12-2043-2020

Haslinger, K., Koffler, D., Schöner, W., & Laaha, G. (2014). Exploring the link between meteorological drought and streamflow: Effects of climate-catchment interaction. *Water Resources Research*, *50*(3), 2468–2487. https://doi.org/10.1002/2013wr015051

Hedges, L. V. (1981). Distribution theory for Glass's estimator of effect size and related estimators. *Journal of Educational Statistics*, *6*(2), 107–128. https://doi.org/10.2307/1164588

Huang, S., Li, P., Huang, Q., Leng, G., Hou, B., & Ma, L. (2017). The propagation from meteorological to hydrological drought and its potential influence factors. *Journal of Hydrology*, *547*, 184–195. https://doi.org/10.1016/j.jhydrol.2017.01.041

Huning, L. S., & AghaKouchak, A. (2020). Global snow drought hot spots and characteristics. *Proceedings of the National Academy of Sciences*, *117*(33), 19753–19759. https://doi.org/10.1073/pnas.1915921117

Janga Reddy, M., & Ganguli, P. (2012). Application of copulas for derivation of drought severity–duration–frequency curves. *Hydrological Processes*, *26*(11), 1672–1685. https://doi.org/10.1002/hyp.8287

Kao, S.-C., & Govindaraju, R. S. (2010). A copula-based joint deficit index for droughts. *Journal of Hydrology*, *380*(1–2), 121–134. https://doi.org/10.1016/j.jhydrol.2009.10.029

Kendon, M., Marsh, T., & Parry, S. (2013). The 2010–2012 drought in England and Wales. *Weather*, *68*(4), 88–95. https://doi.org/10.1002/wea.2101

Koster, R. D., Dirmeyer, P. A., Guo, Z., Bonan, G., Chan, E., Cox, P., et al. (2004). Regions of strong coupling between soil moisture and precipitation. *Science*, *305*(5687), 1138–1140. https://doi.org/10.1126/science.1100217

Krysanova, V., Zaherpour, J., Didovets, I., Gosling, S. N., Gerten, D., Hanasaki, N., et al. (2020). How evaluation of global hydrological models can help to improve credibility of river discharge projections under climate change. *Climatic Change*, *163*(3), 1353–1377. https://doi.org/10.1007/s10584-020-02840-0

Laio, F., Di Baldassarre, G., & Montanari, A. (2009). Model selection techniques for the frequency analysis of hydrological extremes. *Water Resources Research*, *45*(7). https://doi.org/10.1029/2007WR006666

Lehner, B., Döll, P., Alcamo, J., Henrichs, T., & Kaspar, F. (2006). Estimating the impact of global change on flood and drought risks in Europe: A continental, integrated analysis. *Climatic Change*, *75*(3), 273–299. https://doi.org/10.1007/s10584-006-6338-4

Leonard, M., Westra, S., Phatak, A., Lambert, M., van den Hurk, B., McInnes, K., et al. (2014). A compound event framework for understanding extreme impacts. *Wiley Interdisciplinary Reviews: Climate Change*, *5*(1), 113–128. https://doi.org/10.1002/wcc.252

Loon, A. F. V. (2015). Hydrological drought explained. *WIREs Water*, *2*(4), 359–392. https://doi.org/10.1002/wat2.1085

Markonis, Y., & Koutsoyiannis, D. (2016). Scale-dependence of persistence in precipitation records. *Nature Climate Change*, *6*(4), 399–401. https://doi.org/10.1038/nclimate2894

Marsh, T., Cole, G., & Wilby, R. (2007). Major droughts in England and Wales, 1800–2006. *Weather*, *62*(4), 87–93. https://doi.org/10.1002/wea.67

McKee, T. B., Doesken, N. J., & Kleist, J. (1993). The relationship of drought frequency and duration to time scales. *Proceedings of the 8th Conference on Applied Climatology* (Vol. *17*, pp. 179–183).

Mesbahzadeh, T., Mirakbari, M., Mohseni Saravi, M., Soleimani Sardoo, F., & Miglietta, M. M. (2020). Meteorological drought analysis using copula theory and drought indicators under climate change scenarios (RCP). *Meteorological Applications*, *27*(1), e1856. https://doi.org/10.1002/met.1856

Mirabbasi, R., Fakheri-Fard, A., & Dinpashoh, Y. (2012). Bivariate drought frequency analysis using the copula method. *Theoretical and Applied Climatology*, *108*(1), 191–206. https://doi.org/10.1007/s00704-011-0524-7

Najibi, N., & Devineni, N. (2018). Recent trends in the frequency and duration of global floods. *Earth System Dynamics*, *9*(2), 757–783. https://doi.org/10.5194/esd-9-757-2018

Naranjo, L., Glantz, M. H., Temirbekov, S., & Ramírez, I. J. (2018). El Niño and the Köppen–Geiger classification: A prototype concept and methodology for mapping impacts in central America and the circum-caribbean. *International Journal of Disaster Risk Science*, *9*(2), 224–236. https://doi.org/10.1007/s13753-018-0176-7

Nelsen, R. B. (2013). *An introduction to copulas* (Vol. 139). Springer.

Oertel, M., Meza, F. J., Gironás, J., Scott, A. C., Rojas, F., & Pineda-Pablos, N. (2018). Drought propagation in semi-Arid River Basins in Latin America: Lessons from Mexico to the southern cone. *Water*, *10*(11), 1564. https://doi.org/10.3390/w10111564

O'Gorman, P. A., & Schneider, T. (2009). The physical basis for increases in precipitation extremes in simulations of 21st-century climate change. *Proceedings of the National Academy of Sciences*, *106*(35), 14773–14777. https://doi.org/10.1073/pnas.0907610106

Özger, M., Mishra, A. K., & Singh, V. P. (2013). Seasonal and spatial variations in the scaling and correlation structure of streamflow data. *Hydrological Processes*, *27*(12), 1681–1690. https://doi.org/10.1002/hyp.9314

Parry, S., Hannaford, J., Lloyd-Hughes, B., & Prudhomme, C. (2012). Multi-year droughts in Europe: Analysis of development and causes. *Hydrology Research*, *43*(5), 689–706. https://doi.org/10.2166/nh.2012.024

Pettitt, A. N. (1979). A non-parametric approach to the change-point problem. *Journal of the Royal Statistical Society: Series C (Applied Statistics)*, *28*(2), 126–135. https://doi.org/10.2307/2346729

Poonia, V., Jha, S., & Goyal, M. K. (2021). Copula based analysis of meteorological, hydrological and agricultural drought characteristics across Indian River Basins. *International Journal of Climatology*, *41*(9), 4637–4652. https://doi.org/10.1002/joc.7091

Rajsekhar, D., Singh, V. P., & Mishra, A. K. (2015). Hydrologic drought atlas for Texas. *Journal of Hydrologic Engineering*, *20*(7). https://doi.org/10.1061/(ASCE)HE.1943-5584.0001074

Raymond, C., Horton, R. M., Zscheischler, J., Martius, O., AghaKouchak, A., Balch, J., et al. (2020). Understanding and managing connected extreme events. *Nature Climate Change*, *10*(7), 611–621. https://doi.org/10.1038/s41558-020-0790-4

Roundy, J. K., Ferguson, C. R., & Wood, E. F. (2012). Temporal variability of land–Atmosphere coupling and its implications for drought over the southeast United States. *Journal of Hydrometeorology*, *14*(2), 622–635. https://doi.org/10.1175/jhm-d-12-090.1

Sahana, V., Sreekumar, P., Mondal, A., & Rajsekhar, D. (2020). On the rarity of the 2015 drought in India: A country-wide drought atlas using the multivariate standardized drought index and copula-based severity-duration-frequency curves. *Journal of Hydrology: Regional Studies*, *31*, 100727. https://doi.org/10.1016/j.ejrh.2020.100727

Schewe, J., Heinke, J., Gerten, D., Haddeland, I., Arnell, N. W., Clark, D. B., et al. (2014). Multimodel assessment of water scarcity under climate change. *Proceedings of the National Academy of Sciences*, *111*(9), 3245–3250. https://doi.org/10.1073/pnas.1222460110

Sen, Z. (1980). Statistical analysis of hydrologic critical droughts. *Journal of the Hydraulics Division*, *106*(1), 99–115. https://doi.org/10.1061/jyceaj.0005362

Serinaldi, F. (2015). Dismissing return periods. *Stochastic Environmental Research and Risk Assessment*, *29*(4), 1179–1189. https://doi.org/10.1007/s00477-014-0916-1

Sheffield, J., & Wood, E. F. (2007). Characteristics of global and regional drought, 1950–2000: Analysis of soil moisture data from off-line simulation of the terrestrial hydrologic cycle. *Journal of Geophysical Research*, *112*(D17), D17115. https://doi.org/10.1029/2006JD008288

Shiau, J. T. (2006). Fitting drought duration and severity with two-dimensional copulas. *Water Resources Management*, *20*(5), 795–815. https://doi.org/10.1007/s11269-005-9008-9

Shukla, S., & Wood, A. W. (2008). Use of a standardized runoff index for characterizing hydrologic drought. *Geophysical Research Letters*, *35*(2), L02405. https://doi.org/10.1029/2007GL032487

Singh, H., Najafi, M. R., & Cannon, A. J. (2020). Characterizing non-stationary compound extreme events in a changing climate based on large-ensemble climate simulations. *Climate Dynamics*, *56*(24), 1–17. https://doi.org/10.1007/s00382-020-05538-2

Stagge, J. H., Rosenberg, D. E., DeRose, R. J., & Rittenour, T. M. (2018). Monthly paleostreamflow reconstruction from annual tree-ring chronologies. *Journal of Hydrology*, *557*, 791–804. https://doi.org/10.1016/j.jhydrol.2017.12.057

Stahl, K., Tallaksen, L. M., Gudmundsson, L., & Christensen, J. H. (2011). Streamflow data from small basins: A challenging test to high-resolution regional climate modeling. *Journal of Hydrometeorology*, *12*(5), 900–912. https://doi.org/10.1175/2011jhm1356.1

Svoboda, M., Hayes, M., & Wood, D. (2012). *Standardized precipitation index user guide*. World Meteorological Organization Geneva. Retrieved from https://public.wmo.int/en/resources/library/standardized-precipitation-index-user-guide

Tallaksen, L. M., & Van Lanen, H. A. (2004). *Hydrological drought: Processes and estimation methods for streamflow and groundwater*. Elsevier (ISBN: 9780128190821).

Tan, X., & Gan, T. Y. (2015). Nonstationary analysis of annual maximum streamflow of Canada. *Journal of Climate*, *28*(5), 1788–1805. https://doi.org/10.1175/jcli-d-14-00538.1

Trenberth, K. E., Dai, A., van der Schrier, G., Jones, P. D., Barichivich, J., Briffa, K. R., & Sheffield, J. (2014). Global warming and changes in drought. *Nature Climate Change*, *4*(1), 17–22. https://doi.org/10.1038/nclimate2067

Van Dijk, A. I., Beck, H. E., Crosbie, R. S., de Jeu, R. A., Liu, Y. Y., Podger, G. M., et al. (2013). The Millennium Drought in southeast Australia (2001–2009): Natural and human causes and implications for water resources, ecosystems, economy, and society. *Water Resources Research*, *49*(2), 1040–1057. https://doi.org/10.1002/wrcr.20123

Van Loon, A. F. (2015). Hydrological drought explained. *Wiley Interdisciplinary Reviews: Water*, *2*(4), 359–392. https://doi.org/10.1002/wat2.1085

Van Loon, A. F., & Laaha, G. (2015). Hydrological drought severity explained by climate and catchment characteristics. *Journal of Hydrology*, *526*, 3–14. https://doi.org/10.1016/j.jhydrol.2014.10.059

Van Loon, A. F., Tijdeman, E., Wanders, N., Van Lanen, H. a. J., Teuling, A. J., & Uijlenhoet, R. (2014). How climate seasonality modifies drought duration and deficit. *Journal of Geophysical Research: Atmospheres*, *119*(8), 4640–4656. https://doi.org/10.1002/2013jd020383

Wan, W., Zhao, J., Li, H.-Y., Mishra, A., Leung, L. R., Hejazi, M., et al. (2017). Hydrological drought in the Anthropocene: Impacts of local water extraction and reservoir regulation in the U.S. *Journal of Geophysical Research: Atmospheres*, *122*(21), 11313–11328. https://doi.org/10.1002/2017jd026899

Wanders, N., Thober, S., Kumar, R., Pan, M., Sheffield, J., Samaniego, L., & Wood, E. F. (2019). Development and evaluation of a pan-European multimodel seasonal hydrological forecasting system. *Journal of Hydrometeorology*, *20*(1), 99–115. https://doi.org/10.1175/jhm-d-18-0040.1

Wang, F., Wang, Z., Yang, H., Di, D., Zhao, Y., & Liang, Q. (2020). A new copula-based standardized precipitation evapotranspiration streamflow index for drought monitoring. *Journal of Hydrology*, *585*, 124793. https://doi.org/10.1016/j.jhydrol.2020.124793

Wei, J., Su, H., & Yang, Z.-L. (2016). Impact of moisture flux convergence and soil moisture on precipitation: A case study for the southern United States with implications for the globe. *Climate Dynamics*, *46*(1–2), 467–481. https://doi.org/10.1007/s00382-015-2593-2

Winchell, T. S., Barnard, D. M., Monson, R. K., Burns, S. P., & Molotch, N. P. (2016). Earlier snowmelt reduces atmospheric carbon uptake in midlatitude subalpine forests. *Geophysical Research Letters*, *43*(15), 8160–8168. https://doi.org/10.1002/2016gl069769

Wu, J., Miao, C., Zheng, H., Duan, Q., Lei, X., & Li, H. (2018). Meteorological and hydrological drought on the loess plateau, China: Evolutionary characteristics, impact, and propagation. *Journal of Geophysical Research: Atmospheres*, *123*(20), 11569–11584. https://doi.org/10.1029/2018jd029145

Wyżga, B., Radecki-Pawlik, A., Galia, T., Plesiński, K., Škarpich, V., & Dušek, R. (2020). Use of high-water marks and effective discharge calculation to optimize the height of bank revetments in an incised river channel. *Geomorphology*, *356*, 107098. https://doi.org/10.1016/j.geomorph.2020.107098

Yang, L., Franzke, C. L. E., & Fu, Z. (2020). Power-law behaviour of hourly precipitation intensity and dry spell duration over the United States. *International Journal of Climatology*, *40*(4), 2429–2444. https://doi.org/10.1002/joc.6343

Zscheischler, J., Martius, O., Westra, S., Bevacqua, E., Raymond, C., Horton, R. M., et al. (2020). A typology of compound weather and climate events. *Nature Reviews Earth & Environment*, *1*(7), 333–347. https://doi.org/10.1038/s43017-020-0060-z

Zscheischler, J., & Seneviratne, S. I. (2017). Dependence of drivers affects risks associated with compound events. *Science Advances*, *3*(6), e1700263. https://doi.org/10.1126/sciadv.1700263

Zscheischler, J., Westra, S., Hurk, B. J. J. M., van den Seneviratne, S. I., Ward, P. J., Pitman, A., et al. (2018). Future climate risk from compound events. *Nature Climate Change*, *8*(6), 469–477. https://doi.org/10.1038/s41558-018-0156-3